

A NOVELISTIC FRACTAL ANTENNA FOR ULTRA-WIDEBAND (UWB) APPLICATIONS

M. Levy^{1, 2, *}, S. Bose¹, A. Dinh², and D. S. Kumar¹

¹Department of Electronics and Communication Engineering, National Institute of Technology, Trichy, Tamil Nadu-620015, India

²Department of Electrical and Computer Engineering, University of Saskatchewan, Saskatoon-S7N5A9, Canada

Abstract—Fractal arrays are used to increase the bandwidth of the antenna and to reduce grating lobes. The frequency range from 3.1 to 10.6 GHz is specially allocated for the UWB applications. In this paper, a novel antenna based on fractal concepts for ultra wideband (UWB) applications is analyzed, designed, fabricated and tested. Further the antenna is analyzed using the emerging fractal concepts and transmission line method (TLM). The proposed antenna has a good gain bandwidth with broadside radiation pattern. This design is suitable for 3D IC inter-chip and intra-chip communication, and medical imaging applications. This is called Levy's antenna.

1. INTRODUCTION

Microstrip antennas in general consist of a radiating patch on one side of a dielectric substrate ($\epsilon_r \leq 10$) and has a ground plane on the other. The patch conductors, normally of copper or gold, can assume virtually any shape, but conventional and symmetrical shapes are generally used to simplify analysis and performance prediction. Ideally, the dielectric constant of the substrate should be low ($\epsilon_r \sim 2.5$), so as to enhance the fringe fields which account for the radiation [1, 2]. Various types of substrates having a large range of dielectric constants and loss tangents have been developed. Flexible substrates are also available which make it possible to fabricate simple conformal wraparound antennas.

Antenna arrays are commonly used in the design of apertures, which provide benefits such as high gain and agile beam steering capabilities. When designing an antenna array to operate over a wide

Received 7 October 2012, Accepted 2 November 2012, Scheduled 6 November 2012

* Corresponding author: Mounissamy Levy (levy_young@yahoo.com).

bandwidth and over a large scan volume, the conventional approach is to use a lattice where the elements are placed close together in terms of electrical spacing. Because of this, the mutual coupling between the individual radiating elements becomes significant and must be considered during the design of the array. The most robust and effective way to design a dense array is to treat the radiating elements as if they were in an infinite array environment. Radiating elements are typically modeled using some types of full wave computational electromagnetic CAD tools; however the boundary conditions of the model are assumed to be periodic. In this manner, the fields on one side of the model are assumed to be equal to the fields on the other, plus some phase offset associated with the scan of the array. Effective dense UWB array designs include the connected array and the Vivaldi array. In these arrays, the currents are shared between individual apertures, leading to the high levels of mutual coupling in the array. However, there are some difficulties associated with the design of these dense arrays [4–6]. Fractal array design, to an extent, can help solve these problems. Fractal array design is used in this paper to achieve a novel ultra wideband antenna. Recent literature survey [3–27] shows that excellent research results are presented and novel slits and novel structure variations are used to improve the performance of existing antennas and promising results are obtained but the proposed method uses an entirely new concept of fractal design [28] in ultra wideband antenna.

The paper is organized subsequently as follows. Section 2 introduces the fractal concept and discusses on the mathematical prerequisites. Section 3 focuses on the graphical analysis of the array factor and directivity plots for the proposed fractal antenna. Section 4 throws some light on the mathematical analysis of the proposed antenna. Section 5 discusses on the mathematical analysis of the circular disk geometry. Section 6 deals with the Iterated function systems used in the fractal array geometry predominantly for ultra wideband application. Section 7 highlights the novel fractal antenna called Levy's antenna, its analysis and design, fabrication and test results. The paper concludes with Section 8 giving the scope for future work.

2. MATHEMATICAL BACKGROUND FOR FRACTAL ANTENNA

A fractal is a recursively generated object having a fractional dimension. Many objects, including antennas, can be designed using the recursive nature of a fractal. The important properties of fractal

arrays are frequency independent multi band characteristic schemes for realizing low side-lobe designs, systematic approaches to thinning, and the ability to develop rapid beam-forming algorithms by exploiting the recursive nature of fractals. These arrays have fractional dimensions that are found from generating sub array used to recursively create the fractal array [29].

Repetitive application of a generating sub array can form a rich class of fractal array. A generating sub array is a small array at scale one ($P = 1$) where P is the scale factor, and is used to construct larger arrays of higher scales ($P > 1$). The generating sub array elements are turned on and off in a particular pattern in many cases. A set formula for copying, scaling, and translation of the generating sub array is then followed in order to produce the fractal array. Hence, fractal arrays that are created in this manner will compose of a sequence of self-similar sub arrays. In other words, this may be conveniently considered as an array of arrays [29].

The array factor for a fractal array [29] of this type may be expressed in the general form:

$$AF_P(\psi) = \prod_{i=1}^P \hat{G}A(\delta^{i-1}\psi) \quad (1)$$

where $GA(\psi)$ represents the array factor associated with the generating sub array. The parameter δ is a scale or expansion factor that governs how large the array grows with each recursive application of the generating sub array. The expression for the fractal array factor given in Equation (1) is simply the product of scaled versions of a generating sub array factor. Therefore, Equation (1) may be regarded as representing a formal statement of the pattern multiplication theorem for fractal arrays.

One of the more intriguing attributes of fractal arrays is the possibility for developing algorithms, based on the compact product representation of Equation (1), which are capable of performing extremely rapid pattern computations. For example consider a linear array of isotropic elements, uniformly spaced at a distance d apart. The array factor corresponding to this linear array [29] may be expressed in the form:

$$AF(\psi) = I_o + 2 \sum_{n=1}^N I_n \cos \{n\psi\} \quad (2)$$

for odd number of elements [29] and,

$$AF(\psi) = 2 \sum_{n=1}^N I_n \cos \left\{ \left(n - \frac{1}{2} \right) \psi \right\} \quad (3)$$

for even number of elements where n is the total number of elements where,

$$N = \left(\frac{n-1}{2} \right) \quad (4)$$

$$\psi = kd \{ \cos \theta - \cos \theta_o \} \quad (5)$$

$$k = \frac{2\pi}{\lambda} \quad (6)$$

where N is the summation factor, ψ the progressive phase shift, and k the phase constant.

The directivity for fractal array antenna [29] is given by:

$$D_P(u) = \frac{\hat{A}F_P^2\left(\frac{\pi}{2}u\right)}{\frac{1}{2} \int_{-1}^1 \hat{A}F_P^2\left(\frac{\pi}{2}u\right) du} \quad (7)$$

where,

$$\psi = \frac{\pi}{2}u \quad (8)$$

and,

$$u = \cos \theta \quad (9)$$

3. GRAPHICAL ANALYSIS OF ARRAY-FACTOR AND DIRECTIVITY OF FRACTAL ARRAYS

The antenna arrays, as discussed in Section 2, become fractal-like when appropriate elements are turned off, such that, antenna current function varies as:

$$I_n = 1, \text{ if element } n \text{ is turned ON, \&}$$

$$I_n = 0, \text{ if element } n \text{ is turned OFF.}$$

Hence, fractal arrays produced by following this procedure belong to a special category of thinned arrays. If the above equations are used to calculate the array factor for an odd number of elements, then N cosine functions must be evaluated and N additions performed, for each angle. One of the simplest schemes for constructing a fractal linear array follows the recipe of the Cantor set. Cantor linear arrays were first proposed and studied in [30] for their great potential use in the design of low-side lobe arrays.

Starting with a three element generating sub-array, the basic triadic Cantor array may be created by applying it repeatedly over P scales of growth. The generating sub-array in this case has three uniformly spaced elements, with the center element turned off or

removed, i.e., 101. The triadic Cantor array is generated recursively by replacing 1 by 101 and 0 by 000 at each stage of the construction. For example, at the second stage of construction ($P = 2$), the array pattern would look like:

$$1\ 0\ 1\ 0\ 0\ 0\ 1\ 0\ 1$$

In this fashion, the different stages of fractal pattern is grown. The antenna array grows rapidly in size with increment in stage number, and its final pattern depends on the initial stage pattern. The same case can be applied for planar construction also. Current research and investigations on three dimensional fractal arrays is in progress to refine and tailor the pattern of the required beam. Non-linear fractal arrays with non-uniform amplitude and unequal spacing also find application to obtain desired radiation patterns. However with the current example in hand, at the third stage ($P = 3$), we would have:

$$1\ 0\ 1\ 0\ 0\ 0\ 1\ 0\ 1\ 0\ 0\ 0\ 0\ 0\ 0\ 0\ 0\ 0\ 0\ 1\ 0\ 1\ 0\ 0\ 0\ 1\ 0\ 1$$

The array factor of the three-element generating sub-array with the representation 101 is:

$$GA(\psi) = 2 \cos \{\psi\} \tag{10}$$

which may be derived from the array factor equation by setting $N = 1$, $I_o = 0$ and $I_1 = 1$. Substituting this equation into Equation (1) and choosing an expansion factor of 3, results in an expression for the Cantor array factor given by:

$$\hat{A}F_P(\psi) = \prod_{i=1}^P \hat{G}A(3^{i-1}\psi) = \prod_{i=1}^P \cos \{3^{i-1}\psi\} \tag{11}$$

Here the hat notation indicates that the quantities have been normalized. The array factor pattern and the directivity pattern for $P \in \{1, 2, 3, 4\}$ and $\delta = 3$ are shown in Figures 1 to 10.

As both values increases the plot shows improvement in characteristics, the directivity increases and the pattern becomes narrower. Another fantastic advantage is the Equation (11) only

Table 1. Tabulation of the variation of P and δ .

	$P = 1$	$P = 2$	$P = 3$	$P = 4$	$P = 5$
$\delta = 3$	1	2	4	10	24
$\delta = 5$	2	6	20	78	312
$\delta = 7$	3	12	57	300	1680
$\delta = 9$	4	20	121	820	5904

requires P cosine-function evaluations and $P - 1$ multiplication. In the case of an 81 element triadic cantor array, the fractal array factor is at least $N/P = 40/4 = 10$ times faster to calculate than the conventional discrete Fourier transform. The multiband characteristics of linear fractal array are discussed in [31] and [32]. The same procedure can be applied for the Sierpinski carpet arrays for developing efficient algorithms which can be used in planar smart antennas. The multiband characteristics of Sierpinski carpet array is discussed in [31]. More about fractal arrays are discussed in [32]. Details of antenna design techniques are discussed in [33], and particularly about printed antenna design in [34]. The application of these algorithms for rapid beam forming in smart antennas is discussed in [35, 36].

Table 1 shows the increase in speed factor as the values of P and δ varies. As the value of P and δ increases the speed factor increases enormously. For example, with for $P = 4$ & $\delta = 7$ the fractal array

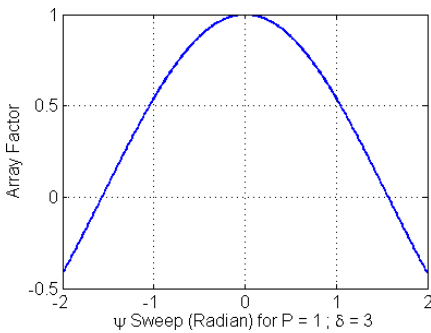


Figure 1. Fractal array factor pattern for $P = 1$; $\delta = 3$.

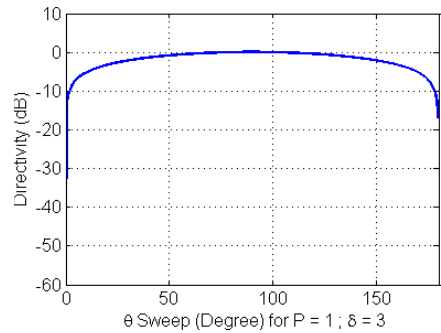


Figure 2. Directivity pattern for $P = 1$; $\delta = 3$.

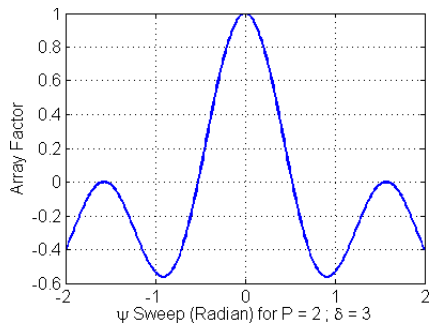


Figure 3. Fractal array factor pattern for $P = 2$; $\delta = 3$.

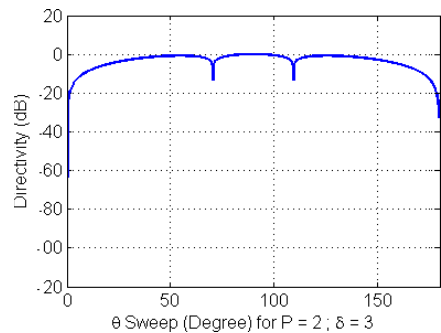


Figure 4. Directivity pattern for $P = 2$; $\delta = 3$.

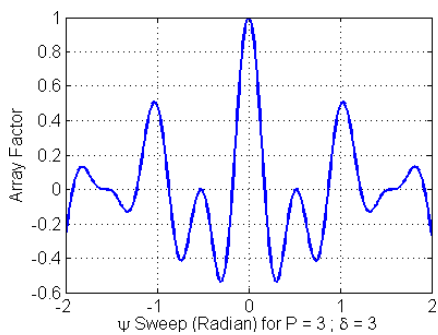


Figure 5. Fractal array factor pattern for $P = 3$; $\delta = 3$.

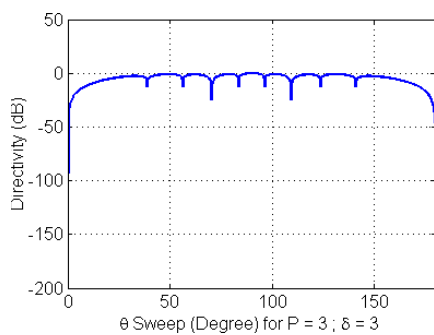


Figure 6. Directivity pattern for $P = 3$; $\delta = 3$.

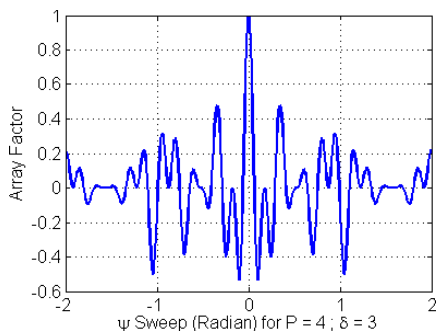


Figure 7. Fractal array pattern for $P = 4$; $\delta = 3$.

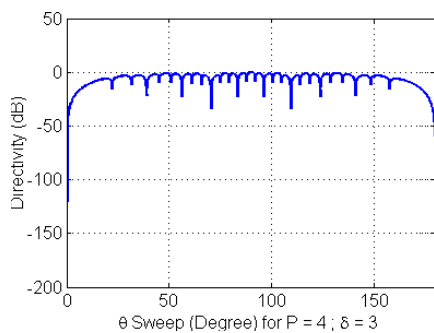


Figure 8. Directivity pattern for $P = 4$; $\delta = 3$.

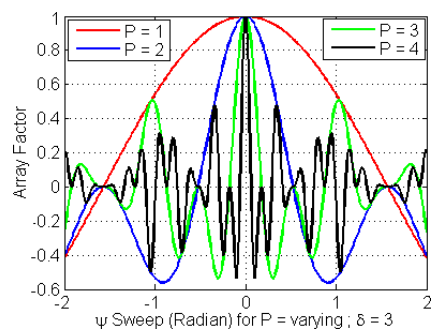


Figure 9. Combined array factor pattern for comparison.

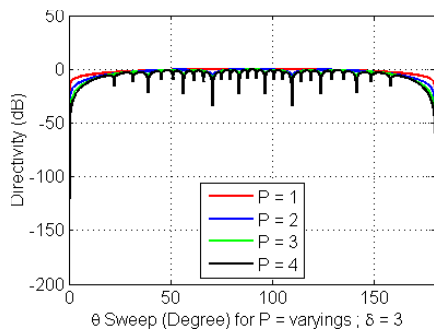


Figure 10. Combined directivity pattern for comparison.

factor is 300 times faster to calculate than the conventional case. This property can be utilized in smart antennas to produce rapid beam forming algorithms [35, 36].

4. MATHEMATICAL ANALYSIS USING FRACTAL CONCEPTS AND TRANSMISSION LINE METHOD (TLM)

The UWB antenna designed uses the fractal concepts and it can be analysed using transmission line method (TLM). The signal emitted from the k^{th} user in impulse radio consists of a large number of subnanosecond pulses [37], expressed as:

$$s^{(k)}(t) = \sum_{j=-\infty}^{\infty} w\left(t - jT_f - c_j^{(k)}T_c - \delta d_{\lfloor j/N_s \rfloor}^{(k)}\right) \quad (12)$$

where $w(t)$ is referred to as the monocycle pulse shape, T_f is the pulse repetition period, $\{c_j^{(k)}\}$ is the time hopping sequence associated with user k , $c_j^{(k)}T_c$ corresponds to the time shift to the j^{th} pulse, T_c is the duration of addressable time delay bins. The data sequence $\{d_j^{(k)}\}$ changes the delay via the modulation index δ , which should be chosen to optimise the performance, N_s monocycles are modulated by a data symbol, and hence the data rate [37] is expressed as:

$$R_s = \frac{1}{N_s T_f} \quad (13)$$

A typical pulse shape for the monocycle is the Gaussian doublet, given by [37], as:

$$w(t) = \left[1 - 4\pi \left(\frac{t}{\tau_m}\right)^2\right] e^{-2\pi \left(\frac{t}{\tau_m}\right)^2} \quad (14)$$

where τ_m is the parameter to determine the frequency characteristic of the Gaussian doublet. Alternatively an ultra-wideband can be created by multicarrier modulation with a large number of carriers. In multi-carrier modulation, the original data sequence is split into many data streams, each of them modulating different parallel carriers, i.e., subcarrier. One of the main requirements for UWB antennas is efficiency and matching which is given by [37], and expressed as:

$$\eta_{rad}(\%) = \frac{\int_0^{\infty} P_t(\omega) \left(1 - |\Gamma_t(\omega)|^2\right) d\omega}{\int_0^{\infty} P_t(\omega) d\omega} \times 100\% \quad (15)$$

where P_t is the power at the terminals of the transmitting antenna and $\Gamma_t(\omega)$ the reflection coefficient normalised to the characteristic impedance Z_o .

The second important requirement for UWB antenna is signal distortion and dispersion (ringing) effect. The UWB antenna deforms the transmitted signal. The antenna response to a pulse of very short duration (as is typical in UWB) is seen as a ripple after the pulse, which is called the ringing effect [37], and expressed as:

$$v_n(t) = \frac{d^n}{dt^n} \cdot \exp \left[- \left(\frac{t}{\sigma} \right)^2 \right] \quad (16)$$

$$\widetilde{v}_n(\omega) = (j\omega)^n \sigma \sqrt{\pi} \exp \left[- \left(\frac{\omega\sigma}{2} \right)^2 \right] \quad (17)$$

where $v_n(t)$ in Equation (16) refers to the ripple function in time domain and $\widetilde{v}_n(\omega)$ in Equation (17) gives the normalized spectrum. σ is the standard deviation of the Gaussian pulse.

The relative bandwidth BW_r [37] is defined as:

$$BW_r = 2 \frac{(f_h - f_l)}{(f_h + f_l)} \quad (18)$$

where f_l is the band's lowest frequency, and f_h is the band's highest frequency.

In this case, it is desirable for the antenna's transfer function to be as constant as possible over the desired frequency, so that it does not affect the pulse. Due to their unique properties of time and spectrum, the Rayleigh family of pulses (derivatives of different orders of the Gaussian pulse) is widely used as signal sources for UWB systems. The corresponding equations in the time and frequency domains are given by [37], as:

$$v_n(t) = \text{square of the } n^{\text{th}} \text{ derivative of } \frac{d}{dt} \exp \left[- \left(\frac{t}{\sigma} \right)^2 \right] \quad (19)$$

5. ANALYSIS OF CIRCULAR DISC MONOPOLE UWB ANTENNA USED IN LEVY'S ANTENNA

For circular disc monopole, the ground plane serves as an impedance matching circuit. Consequently it tunes the input impedance and hence the 10 dB return loss bandwidth by changing the feed gap h . Another two important design parameters that affect the antenna performance are the width of the ground plane W , and the dimension of the disc. The effects of these two parameters can be well explained

by investigating the current distributions of the antenna. Circular geometries offer performance at par to that of rectangular geometries. In some applications circular geometries offer certain advantages over other configurations. Recent experimental results [38] have shown that circular disk microstrip elements may be easily modified to produce arranged impedances, radiation patterns, and frequencies of operation.

The basic disk antenna geometry comprises of a thin, conducting circular patch on a dielectric substrate backed by ground plane. The electric field within the substrate has essentially only a z -component, and the magnetic field has essentially x and y components. Because $h \ll \lambda_o$, the fields do not vary along the z direction, and the component of the current normal to the edge of the microstrip approaches zero at the edge. This implies that the tangential component of the magnetic field at the edge is vanishingly small. With these assumptions, the micro strip disk can be modeled as a cylindrical cavity, bounded at its top and bottom by electric walls and on its sides by a magnetic wall. Thus the fields within the dielectric region of the micro strip, corresponding to TM_{nm} modes, may be determined by solving a cavity problem. The simple cavity model may be extended to include the feed source. The considerations for the cavity itself are the same as those discussed for the simple cavity model. In modal expansion model the total field of a probe-excited cavity is expanded in terms of mode vectors. The orthonormal electric field mode vectors corresponding to TM modes for non-radiating circular cavity equations are solved. The wire grid model consists of selecting a grid configuration compatible with the currents on the micro strip element. This method is cumbersome and excessively demanding in terms of computing time. By the Green's function method [42], the input impedance of a circular disk micro strip antenna is calculated and the equivalent impedance boundary conditions. The closed form expression of input impedance is convenient for optimizing various design parameters such as impedance matching and the bandwidth. Consider a circular disk antenna fed by a line source $I_o(z')$ located at (ρ_o, φ_o) in a cylindrical coordinate system (ρ, ϕ, z) . The input impedance Z_{in} may be expressed as [39]

$$Z_{in} = \frac{-1}{I_o(0) I_o^*(0)} \iint E_z(r') J^*(r') ds \quad (20)$$

where $J(r')$ is the surface current on the center conductor of a coaxial line feed, and integration is over the feed surface. The asterisk signifies complex conjugation. To a first order approximation [40], the effect of the diameter of the center conductor may be ignored and equation reduces to:

$$Z_{in} = \frac{-1}{I_o(0) I_o^*(0)} \int_0^h E(z') I_o^*(z') dz' \quad (21)$$

The electric field for the TM_{nm} modes with no variation of fields in the z direction, may be written [41] as:

$$E_z = j\omega\mu I_o(0) G(\rho, \varphi; \rho_0, \varphi_0) \tag{22}$$

where G is Green's function given by [42]:

$$G = \sum_{n=1}^{\infty} \frac{\cos n\varphi \cos n\varphi_0}{\pi} \frac{y_1(\rho) y_2(\rho_0)}{\rho_o [y_1(\rho) y_2'(\rho) - y_1'(\rho) y_2(\rho)]} \tag{23}$$

and $y_1 = J_n(k\rho)$, $y_2 = J_n(k\rho) + A_n Y_n(k\rho)$. The prime sign in the denominator of equation signifies the derivative. The constant A_n is chosen to satisfy the boundary conditions.

$$E_z = 0 \text{ at } \rho = 0 \tag{24}$$

$$-\eta_o \frac{H_\varphi}{E_z} = \frac{\eta_o}{Z_r} = p \text{ at } \rho = a \tag{25}$$

where Z_r represents the impedance boundary condition, and ρ is the normalized admittance. After applying the above boundary conditions, the expression for the input impedance equation [42] reduces to:

$$Z_{in} = \frac{-j\omega h\mu}{2} \sum_{n=1}^{\infty} \left[\frac{J_n^2(k\rho_o)}{A_n} + J_n(k\rho_o) + Y_n(k\rho_o) \right] \tag{26}$$

where

$$A_n = -\frac{pJ_n(ka) - jJ_n'(ka)}{pY_n(ka) - jY_n'(ka)} \tag{27}$$

and

$$p = \eta_o(G_a + jB_a) \tag{28}$$

$$G_a = \frac{2P_T}{h^2 E_o^2 J_n^2(Ka)} \tag{29}$$

$$B_a = \frac{\epsilon\omega\pi a^2}{h} \left[\left\{ 1 + \frac{2h}{\pi a\epsilon_r} \left(\ln\left(\frac{\pi a}{2h}\right) + 1.7726 \right) \right\}^{\frac{1}{2}} - 1 \right] \tag{30}$$

This method provides reasonably good agreement between calculated and measured input impedances.

The annular antenna geometry comprises of a ring shaped strip conductor on one side of a dielectric substrate backed by a ground plane. The solutions for the fields can be obtained by using the cavity model in which the annulus is surrounded by magnetic walls. Since $h \ll \lambda_o$, there is no variation of electric field in the z direction and the fields can be assumed to be TM . For TM_{nm} modes the electric

and magnetic field distributions for a ring resonator in the cylindrical coordinate system (ρ, ϕ, z) are given by [43], as:

$$E_z = E_o [J_n(k\rho) + Y'_n(ka) - J'_n(ka) + Y_n(k\rho)] \cos n\phi \quad (31)$$

$$H_\rho = \frac{j\omega\epsilon}{k^2\rho} \frac{\partial E_z}{\partial\phi} \quad (32)$$

$$H_\phi = \frac{-j\omega\epsilon}{k^2} \frac{\partial E_z}{\partial\rho} \quad (33)$$

where J_n and Y_n are Bessel functions of the first and second kind and of order n , respectively. The prime sign signifies derivatives of the Bessel functions, ϵ is the permittivity of the dielectric and $k = 2\pi\sqrt{\epsilon_r}/\lambda_o$ where ϵ_r is the relative permittivity and λ_o is the free space wavelength. The integer n denotes the azimuth mode number, and the integer m denotes the variation of the fields across the width of the ring.

A circular disk operating in the dominant mode is the most prevalent circular micro strip antenna configuration. The first design step is to select a suitable substrate of appropriate thickness. While bandwidth and radiation efficiency increases with substrate thickness, excess thickness is also undesirable, especially when it is desirable for the antenna to have a low profile and be conformal. The three most commonly used substrate materials are FR4, RT/duroid and Rexolite. For a known dielectric substrate at a specified operating frequency the radius of the micro strip disk element is given by [44]:

$$a = \frac{K}{\left[\left\{ 1 + \frac{2h}{\pi K \epsilon_r} \left(\ln \left(\frac{\pi K}{2h} \right) + 1.7726 \right) \right\}^{\frac{1}{2}} \right]} \quad (34)$$

where

$$K = \frac{8.794}{f_r \sqrt{\epsilon_r}} \quad (35)$$

and f_r is in GHz. The effect of substrate thickness is insignificant for frequencies less than 2 GHz. A reasonably accurate evaluation of the input impedance of a micro strip antenna is necessary to provide a good match between the radiating element and the feed point. Equation (26) provides a reasonably simple basis for calculating the input impedance of a disk antenna for any coaxial feed location. For a micro strip fed element this relation may be used with $X_L = 0$.

The antenna efficiency, defined as the ratio of the radiated power to the input power may be expressed as

$$\eta\% = \frac{P_r}{P_T} X 100 \quad (36)$$

In this case [45], it is:

$$\eta\% = \frac{100(ak_oh)^2 I_1}{(ak_oh)^2 I_1 + 0.953X - 10^6 f^{-3/2} + 0.452h \tan \delta / f} \tag{37}$$

where f is in GHz and h is in meters. The efficiency increases with increasing substrate thickness and decreasing dielectric constant. In an advanced wireless system, an antenna is usually required to enhance the radiation energy in some direction and suppress it in others at certain frequencies. Thus the antenna must also be directional in addition to being a transition device.

The bandwidth of a microstrip antenna is defined as the frequency range over which the value of the input VSWR increases from unity to a tolerable limit value, s . the bandwidth of such antennas may be expressed as:

$$BW = \frac{s - 1}{Q_T \sqrt{s}} \tag{38}$$

where Q_T is the quality factor.

The greater bandwidth is possible by choosing a thicker substrate of low dielectric constant material. The directivity of an antenna is defined as the ratio of the power density in the main beam to the average power density. The directivity of a circular disk antenna excited in the dominant mode ($n = 1$) may be expressed as [46]:

$$D = \frac{\frac{1}{2} \text{Re}(E_\theta H_\varphi^* - E_\varphi H_\theta^*)|_{\theta=0}}{P_r / 4\pi r^2} \tag{39}$$

$$H_\varphi = \frac{E_\theta}{\eta_o} \tag{40}$$

A disk antenna on an alumina substrate has a directivity of about 3.5, which is almost independent of substrate thickness h of 0.1275 cm and operating at resonant frequency. A disk antenna designed using RT/duroid substrate has a maximum directivity of about 5.3 which decreases with increasing resonant frequency and dielectric thickness. The effective gain of the antenna may be calculated from:

$$G_e = \eta D \tag{41}$$

The polarization of a disk element is linear, as is the case for rectangular microstrip antennas. Much of the work about microwave antenna analysis, design and fabrication is available in the textbooks [45–58].

6. ITERATED FUNCTION SYSTEMS (IFS) IN FRACTAL ANTENNAS

IFS are powerful mathematical toolsets that are used to construct a broad spectrum of fractal geometries. These IFS are constructed from a finite set of contraction mappings, each based on an affine linear transformation performed in the Euclidean plane. The most general representation of an affine linear transformation ω_n consists of six real parameters $(a_n, b_n, c_n, d_n, e_n, f_n)$ [28] and is defined as:

$$\begin{pmatrix} x' \\ y' \end{pmatrix} = \omega_n \begin{pmatrix} x \\ y \end{pmatrix} = \begin{pmatrix} a_n & b_n \\ c_n & d_n \end{pmatrix} \begin{pmatrix} x \\ y \end{pmatrix} + \begin{pmatrix} e_n \\ f_n \end{pmatrix} \quad (42)$$

$$w_n(x, y) = (a_n x + b_n y + e_n, c_n x + d_n y + f_n) \quad (43)$$

The parameters of the IFS are often expressed using the compact notation:

$$\begin{pmatrix} a_n & b_n & e_n \\ c_n & d_n & f_n \end{pmatrix} \quad (44)$$

where coordinates x and y represent a point belonging to an initial object, and coordinates x' and y' represent a point belonging to the transformed object. This general transformation can be used to scale rotate, shear, reflect and translate any arbitrary object. The parameters a_n, b_n, c_n and d_n control rotation and scaling while e_n and f_n control linear translation. Consider a set of N affine linear transformations $\omega_1, \omega_2, \omega_3, \omega_4 \dots \omega_N$. This set of transformations forms an IFS that can be used to construct a fractal of stage $\ell + 1$ from a fractal of stage ℓ , given by [28], as:

$$F_{\ell+1} = W(F_\ell) = \cup_{n=1}^N w_n(F_\ell) \quad (45)$$

where W is the Hutchinson operator and F_ℓ is the Fractal of stage ℓ . The pattern produced by the Hutchinson operator is referred to as the generator of the fractal structure. If each transformation reduces the size of the previous object, then the Hutchinson operator can be applied an infinite number of times to generate the final fractal geometry, F_∞ . For example, if set F_0 represents the initial geometry, then this iterative process would yield a sequence of Hutchinson operators that converge upon the final fractal geometry F_∞ .

$$F_1 = W(F_0), F_2 = W(F_1), \dots, F_{k+1} = W(F_k), \dots \quad (46)$$

and,

$$F_\infty = W(F_\infty) \quad (47)$$

If the IFS is truncated at a finite number of stages L , then the object generated is said to be a pre-fractal image, which is often

described as a fractal of stage L . The IFS code for generating an inverted Sierpinski Gasket is shown in Table 2 and the IFS code and associated connection factors for Sierpinski-Based Poly-fractal Geometries is shown in Table 3.

The IFS approach is the most common method used to construct deterministic fractal array geometries; however, deterministic fractals may not resemble natural objects very closely because of their perfect symmetry and order. On the other hand random fractals more closely resemble natural objects because their objects are often created using purely stochastic means. However these objects are difficult to work with especially in the context of optimization, because their structures cannot be recreated with exact precision. In an effort to bridge the gap between deterministic and random fractals a specialized type of fractal geometry called a fractal random tree was developed. This new construct combines together properties of both deterministic and random fractal geometries. Therefore a more generalized expansion of deterministic fractal based geometry is introduced, called poly-fractal geometry. In order to construct a poly-fractal the IFS technique introduced must be expanded to handle multiple generators. Poly-fractal arrays are constructed from multiple generators, $1, 2, \dots, M$, each of which is having a corresponding

Table 2. IFS code for generating an inverted Sierpinski Gasket.

w	a	b	c	d	e	f
1	1/2	0	0	1/2	0	$\sqrt{3}/4$
2	1/2	0	0	1/2	1/2	$\sqrt{3}/4$
3	1/2	0	0	1/2	1/4	0

Table 3. IFS code and associated connection factors for Sierpinski-Based Poly-fractal Geometries.

	w	a	b	c	d	e	f	:	κ
Generator 1	1	1/2	0	0	1/2	0	$\sqrt{3}/4$:	1
	2	1/2	0	0	1/2	1/2	$\sqrt{3}/4$:	1
	3	1/2	0	0	1/2	1/4	0	:	2
Generator 2	1	1/2	0	0	1/2	0	$\sqrt{3}/4$:	2
	2	1/2	0	0	1/2	1/2	$\sqrt{3}/4$:	1
	3	1/2	0	0	1/2	1/4	0	:	2
	4	1/2	0	0	-1/2	1/4	$\sqrt{3}/2$:	1

Hutchinson operator $W_1, W_2, W_3, \dots, W_M$. Each Hutchinson operator W_m in turn contains N_m affine linear transformations,

$$W_m \in \omega_{m,1}, \omega_{m,2}, \omega_{m,3}, \dots, \omega_{m,N_m} \quad (48)$$

The classic theory of solving linear radiating elements involves the study of current distribution. These studies often assume a sinusoidal current distribution. One of the ways to increase bandwidth, which is an absolute requirement for UWB technology, is to widen the conductor. In order to understand how any changes in the geometry of the antenna will affect its behavior, knowledge of current distribution in this situation is vitally important [28].

7. LEVY'S ANTENNA

Using the above concepts and principles, the antenna is analyzed, designed, constructed and tested. Latest research development in UWB antennas focuses on introducing some novel structures and slits in the existing structures to get some improvement by introducing certain changes in design parameters. However, Levy's antenna, as shown in Figure 11, completely implements the new concept of fractal array structure for UWB antenna design. The design parameters are not explicitly discussed as the design may go through patent filing. The antenna is simulated using CST microwave studio CAD tool and all the aspects showed promising results for UWB applications. The conventional fractal approach uses the same basic cell or structure, while the number of cell or elements and the stages of growth are varied,

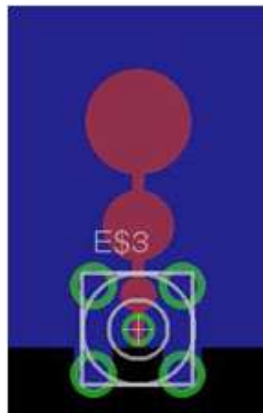


Figure 11. Levy's antenna analyzed and designed using Fractal Concepts.

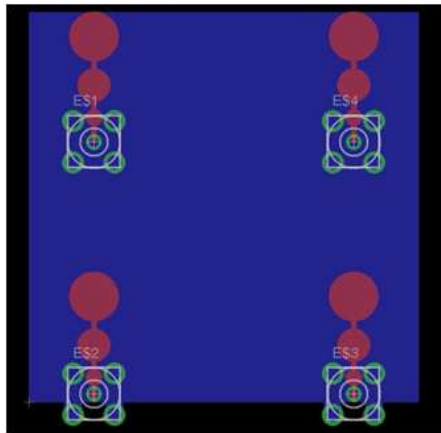


Figure 12. The antenna PCB Layout in EAGLE (Easily Applicable Graphics Layout Editor).

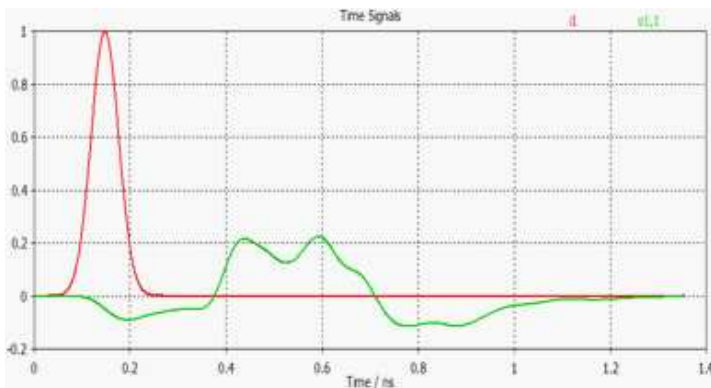


Figure 13. Input/Output relation obtained in CST Microwave studio.

as shown in Figure 12. However, the introduced novel method utilizes the variation in the basic structure or cell as the stages of growth are increased. This is a new approach which is not found in the recent literature surveys and not reported in literatures so far, to the best of the author's knowledge. The antenna is fabricated and tested in the laboratory and the practical results and simulation results are verified.

The input output relation obtained from CST Microwave studio simulation is shown in Figure 13. There is a small variation in time delay between input and output due to the propagation delay of the phase center. The single structure can be viewed as three elements

in the fractal concept with stages of growth along with incremental element size and the analysis can be done using the formulas reported for fractal antennas. The circular array generator concept can be used in this technique but along with increase in the stage, the element size also has to be increased. The first element radius is R and the second element radius is $2R$, the third element size is $3R$ and so on. As long as the stage increases the element radius also increases. The elements can be thought of fed from successive series feed one element behind the other or it can be thought of as three elements fed parallelly and connected to a single source at the feed point.

The impedance variation is shown in the smith chart in Figure 14. The larger the circle implies higher the variation. Research can be done in the direction of getting a small impedance variation circle. Novel metamaterial structures can be used to achieve this purpose. The fabricated antenna is shown in Figure 15.

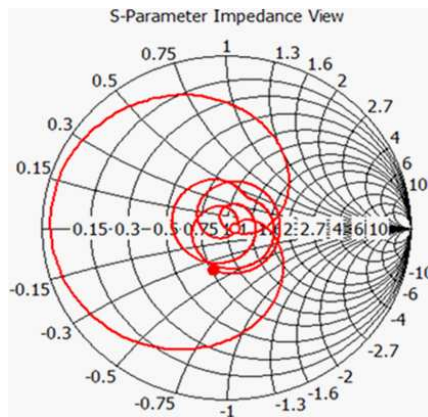


Figure 14. Smith chart Impedance pattern obtained in CST Microwave Studio.

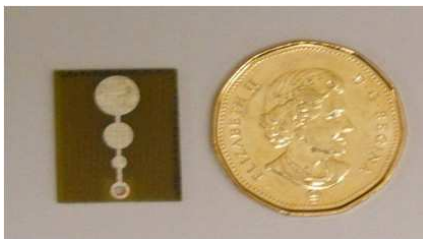


Figure 15. Levy's antenna front view, constructed with finite ground plane.



Figure 16. S_{11} parameter view in the HP agilent network analyzer 8722ES 50 MHz–40 GHz.

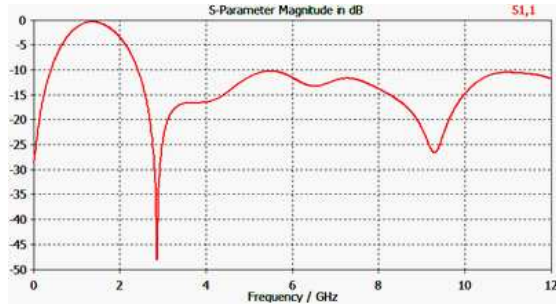


Figure 17. S_{11} parameter from CST Microwave Studio.

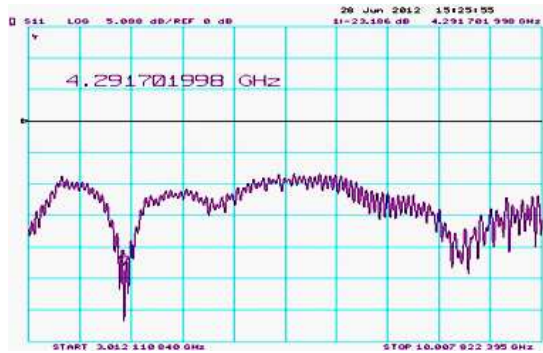


Figure 18. Measured S_{11} parameter from Network analyzer.

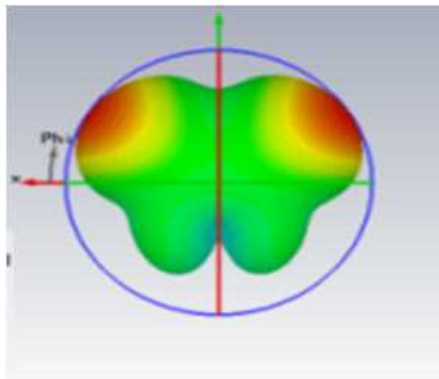


Figure 19. The designed antennas broadside radiation pattern obtained from CST microwave studio.

However, for the example in discussion, the antenna is constructed in two stages, first one with single element and the second with multiple elements in order to achieve arraying. Also finite ground structure and infinite ground structures are constructed but the analyzing and design formulas are different for both structures. The input impedance, feed point, feed method are carefully analyzed and fixed to get the maximum desirable performance. The network analyzer is calibrated using the standard tool kit and then the antenna under test is connected and analyzed. Anechoic chamber is preferred for antenna measurements to avoid reflections. However, the antenna is tested in normal operating conditions to get realistic performance. All the required parameters are analyzed and satisfactory results are obtained, as depicted in Figures 16, 17, 18, and 19.

8. CONCLUSION

A novel printed circular monopole antenna using fractal concepts is analyzed, designed, constructed and tested for ultra wideband (UWB) applications. The characteristics obtained are suited for UWB applications. The theoretical and practical results coincide well and the antenna is radiating in broadside direction. Promising bandwidth impedance matching is obtained over the desired frequency range. The antenna is small in size compared to existing antennas reported in recent literatures. The results obtained are promising and the antenna can be used in applications such as 3D IC wireless communication and medical imaging. The mathematical analysis is performed using fractal concepts and Transmission Line Method (TLM). The theoretical and practical results are verified for their consistency with each other. Further research is elicited towards the reduction of antenna size, including novel materials while improving the desired parameters and performances.

ACKNOWLEDGMENT

The author thanks Searge Nazeranko, Mohammad Raashid, David Klymshyn and Alex Wubo of University of Saskatchewan, Canada. Special thanks goes out to Jack from Telecommunications and Research lab (TR Labs). Further the primary author thanks the Canadian Government and Indian Government for the Award of Canadian Commonwealth Scholarship.

REFERENCES

1. Federal Communications Commission (FCC), "Revision of Part 15 of the commissions's rules regarding ultra-wideband transmissions systems," First Report and Order, 98–153, ET Docket, 2002.
2. Win, M. Z. and R. A. Scholtz, "Impulse radio: How it works," *IEEE Communications Letters*, Vol. 2, 36–38, 1998.
3. Akhoondzadeh-Asl, L., M. Fardis, A. Abolghasemi, and G. R. Dadashzadeh, "Frequency and time domain characteristic of a novel notch frequency UWB antenna," *Progress In Electromagnetics Research*, Vol. 80, 337–348, 2008.
4. Chen, D. and C.-H. Cheng, "A novel compact ultra-wideband (UWB) wide slot antenna with via holes," *Progress In Electromagnetics Research*, Vol. 94, 343–349, 2009.
5. Fallahi, R., A. A. Kalteh, and M. G. Roozbahani, "A novel UWB elliptical slot antenna with band-notched characteristics," *Progress In Electromagnetics Research*, Vol. 82, 127–136, 2008.
6. Lee, J. N. and J. K. Park, "Compact UWB chip antenna design using the coupling concept," *Progress In Electromagnetics Research*, Vol. 90, 341–351, 2009.
7. Zhang, G.-M., J.-S. Hong, and B.-Z. Wang, "Two novel band-notched UWB slot antennas FED by microstrip line," *Progress In Electromagnetics Research*, Vol. 78, 209–218, 2008.
8. Malekpoor, H. and S. Jam, "Ultra-wideband shorted patch antennas FED by folded-patch with multi resonances," *Progress In Electromagnetics Research B*, Vol. 44, 309–326, 2012.
9. Reddy, G. S., S. K. Mishra, S. Kharche, and J. Mukherjee, "High gain and low cross-polar compact printed elliptical monopole UWB antenna loaded with partial ground and parasitic patches," *Progress In Electromagnetics Research B*, Vol. 43, 151–167, 2012.
10. Tilanthe, P., P. C. Sharma, and T. K. Bandopadhyay, "A monopole microstrip antenna with enhanced dual band rejection for UWB applications," *Progress In Electromagnetics Research B*, Vol. 38, 315–331, 2012.
11. Jusoh, M., M. F. B. Jamlos, M. R. B. Kamarudin, and M. F. B. A. Malek, "A MIMO antenna design challenges for UWB application," *Progress In Electromagnetics Research B*, Vol. 36, 357–371, 2012.
12. Lin, S., L.-Z. Wang, Y. Wang, X.-Y. Zhang, and H.-J. Zhang, "Design and analysis of a circular polarization microstrip antenna with koch fractal edges," *Progress In Electromagnetics Research Letters*, Vol. 34, 9–19, 2012.

13. Gomez-Nuñez, E., H. Jardon-Aguilar, J. A. Tirado-Mendez, and R. Flores-Leal, "Ultra-wideband slotted disc antenna compatible with cognitive radio applications," *Progress In Electromagnetics Research Letters*, Vol. 34, 53–63, 2012.
14. Pouyanfar, N. and S. Ahdi Rezaeieh, "Compact UWB antenna with inverted hat shaped resonator and shortening via pins for filtering properties," *Progress In Electromagnetics Research Letters*, Vol. 33, 187–196, 2012.
15. Hayouni, M., A. El Oualkadi, F. Choubani, T. H. Vuong, and J. David, "Antenna ultra wideband enhancement by non-uniform matching," *Progress In Electromagnetics Research Letters*, Vol. 31, 121–129, 2012.
16. Zhang, S.-M., F.-S. Zhang, W.-Z. Li, T. Quan, and H.-Y. Wu, "A compact UWB monopole antenna with wimax and WLAN band rejections," *Progress In Electromagnetics Research Letters*, Vol. 31, 159–168, 2012.
17. Xu, F., L. Tang, X. Chen, and X.-A. Wang, "Active UWB printed antenna with tunable and switchable band-notched functions," *Progress In Electromagnetics Research Letters*, Vol. 30, 21–28, 2012.
18. Jiang, W., et al., "A novel UWB antenna with dual notched bands for WiMAX and WLAN applications," *IEEE Antennas and Wireless Propagation Letters*, 2011.
19. Heong, O. K., et al., "Circuit modeling for rectangular printed disc monopole antenna with slot for UWB system," *Third International Conference on Intelligent Systems Modelling and Simulation*, 2012.
20. Ghavamani, M., L. B. Michael, and R. Kohno, *Ultra Wideband Signals and Systems in Communication Engineering*, 2nd Edition, Wiley, New York, 2008.
21. Vaughan, R. and J. B. Andersen, "Channels, propagation and antennas for mobile communications," Institution of Electrical Engineers, London, 2003.
22. Chen, Z. N., X. H. Wu, H. F. Li, N. Yang, and M. Y. W. Chia, "Considerations for source pulses and antennas in UWB radio systems," *IEEE Transactions on Antennas and Propagation*, Vol. 52, No. 7, 1739–1748, 2004.
23. Gianvittorio, J. P. and Y. Rahmat-Samii, "Fractal antennas: A novel antenna miniaturization technique, and applications," *IEEE Antennas and Propagation Magazine*, Vol. 44, No. 1, 20–36, Feb. 2002.

24. Best, S. R., "The fractal loop antenna: A comparison of fractal and non-fractal geometries," *IEEE Antennas and Propagation Society International Symposium*, Vol. 3, 2001.
25. Werner, D. H. and S. Ganguly, "An overview of fractal antenna engineering research," *IEEE Antennas and Propagation Magazine*, Vol. 45, No. 1, 38–57, Feb. 2003.
26. Kim, Y. and D. L. Jaggard, "The fractal random array," *Proceedings of the IEEE*, Vol. 74, No. 9, 1278–1280, 1986.
27. Lakhtakia, A., N. S. Holter, and V. K. Varadan, "Self-similarity in diffraction by a self-similar fractal screen," *IEEE Transactions on Antennas and Propagation*, Vol. 35, 2, 236–239, Feb. 1987.
28. Gross, F. B., Editor-in-chief, *Frontiers in Antennas: Next Generation Design & Engineering*, McGraw-Hill, New York, 2011.
29. Werner, D. H., R. L. Haupt, and P. L. Werner, "Fractal antenna engineering: The theory and design of fractal antenna arrays," *IEEE Antennas and Propagation Magazine*, Vol. 41, No. 5, Oct. 1999.
30. Liang, X., W. Zhenson, and W. Wenbing, "Synthesis of fractal patterns from concentric-ring arrays," *IEEE Elec. Letters*, Oct. 1996.
31. Baliarda, C. P. and R. Pous, "Fractal design of multiband and low side-lobe arrays," *IEEE Transactions on Antennas and Propagation*, May 1996.
32. Mandelbrot, B. B., *The Fractal Geometry of Nature*, W. H. Freeman and Company, New York, 1983, ISBN: 978-0716711865.
33. Rudge, A. W., et al., Editors, *The Handbook of Antenna Design*, P. Peregrinus on behalf of the Institution of Electrical Engineers, London, 1982–1983.
34. Waterhouse, R., Editor, *Printed Antennas for Wireless Communications*, Wiley, Chichester, England; Hoboken, NJ, 2007.
35. Levy, M., et al., "Rapid beam forming in smart antennas using smart-fractal concepts employing combinational approach algorithms," *International Journal on Antennas and Propagation*, Vol. 2012, Oct. 2012.
36. Levy, M., D. S. Kumar, A. Dinh, and S. Bose, "A novelistic approach for rapid beam forming in smart antennas for wireless applications using smart-fractal concepts and new algorithm," *International Conference on Advances in Mobile Network, Communication and its Applications, (MNCAPPS)*, 5–10, Aug. 1–2, 2012, doi: 10.1109/MNCApps.2012.7.
37. Valderas, D., et al., *Ultra Wideband Antennas*, Imperial College

- Press, 2011.
38. Jian, X., et al., "Study of a printed circular disc monopole antenna for UWB systems," *IEEE Transactions on Antennas and Propagation*, Vol. 53, No. 11, Nov. 2005.
 39. Stutzman, W. L., *Antenna Theory and Design*, John Wiley & Sons, New York, 1998.
 40. Connor, F. R., *Antennas*, E. Arnold, London, 1989.
 41. Marcuvitz, N., *Waveguide Handbook*, P. Peregrinus on behalf of the Institution of Electrical Engineers, London, UK, 1986.
 42. Johnson., R. C., *Designer Notes for Microwave Antennas*, Artech House, Boston, 1991.
 43. Bhartia, P., K. V. S. Rao, and R. S. Tomar, *Millimeter-wave Microstrip and Printed Circuit Antennas*, Artech House, Boston, 1991.
 44. Bahl, I. J. and P. Bhartia., *Microstrip Antennas*, Artech House, Norwood, MA, 1980.
 45. Balanis, C. A., *Antenna Theory: Analysis and Design*, Harper & Row, New York, Toronto, 1982.
 46. Hansen, R. C., Editor., *Moment Methods in Antennas and Scattering*, Artech House, Boston, 1990.
 47. Kuecken, J. A., *Exploring Antennas and Transmission Lines by the Personal Computer*, Van Nostrand Reinhold, New York, 1986.
 48. Fujimotom, K., et al., *Small Antennas*, Letchworth, Hertfordshire, Research Studies Press, England; Wiley, New York, 1987.
 49. Lee, K. F., *Principles of Antenna Theory*, Wiley, Chichester, West Sussex; Wiley, New York, 1984.
 50. Silver, S., Editor, *Microwave Antenna Theory and Design*, P. Peregrinus on behalf of the Institution of Electrical Engineers, London, UK, 1984.
 51. Carr, J. J., *Practical Antenna Handbook*, TAB Books, New York, 1994.
 52. Chatterjee, R., *Antenna Theory and Practice*, Wiley, New York, 1988.
 53. Burberry, R. A., *VHF and UHF Antennas*, P. Peregrinus on behalf of the Institution of Electrical Engineers, London, 1992.
 54. Griffiths, J., *Radio Wave Propagation and Antennas: An Introduction*, Prentice-Hall, Englewood Cliffs, N.J., 1987.
 55. James, J. R., P. S. Hall, and C. Wood, *Microstrip Antenna: Theory and design*, Peter Peregrinus on behalf of the Institution of Electrical Engineers, London, New York, 1981.

56. Weeks, W. L., *Antenna Engineering*, McGraw-Hill, New York, 1968.
57. Wolff, E. A., *Antenna Analysis*, Artech House, Norwood, MA, 1988.
58. Wait, J. R., *Introduction to Antennas & Propagation*, P. Peregrinus on behalf of the Institution of Electrical Engineers, London, U.K., 1986.